

Journal of Electronic Imaging

JElectronicImaging.org

Kernel estimation for robust motion deblurring of noisy and blurry images

Shijie Sun
Huaici Zhao
Bo Li
Mingguo Hao
Jinfeng Lv



Shijie Sun, Huaici Zhao, Bo Li, Mingguo Hao, Jinfeng Lv, "Kernel estimation for robust motion deblurring of noisy and blurry images," *J. Electron. Imaging* **25**(3), 033019 (2016), doi: 10.1117/1.JEI.25.3.033019.

Kernel estimation for robust motion deblurring of noisy and blurry images

Shijie Sun,^{a,b,c,d,*} Huaici Zhao,^{a,c,d} Bo Li,^{a,b,c,d,e} Mingguo Hao,^{a,c,d} and Jinfeng Lv^{a,b,c,d}

^aShenyang Institute of Automation, Chinese Academy of Sciences, No. 114, Nanta Street, Shenhe District, Shenyang City 110016, China

^bUniversity of Chinese Academy of Science, No. 19, Yuquan Road, Shijingshan District, Beijing City 100049, China

^cChinese Academy of Sciences, Key Laboratory of Optical-Electronics Information Processing, No. 114, Nanta Street, Shenhe District, Shenyang City 110016, China

^dKey Laboratory of Image Understanding and Computer Vision, No. 114, Nanta Street, Shenhe District, Shenyang City 110016, China

^eShenyang Institute of Engineering, College of Information, No. 18, Puchang Road, Shenbei New Area, Shenyang City 110136, China

Abstract. Most state-of-the-art single image blind deblurring techniques are still sensitive to image noise, leading to serious performance degradation in their blur kernel estimation when the input image noise increases. We found that reliable kernel estimation could not be given by directly using denoising and existing deblurring algorithms in many cases. We focus on how to estimate a good blur kernel from a noisy blurred image via using the image structure. First, we applied denoising as a preprocess to remove the input image noise and then computed salient image structure of the denoised result based on the total variation model. We also applied a gradient selection method to remove those salient edges that have a possible adverse effect on blur kernel estimation. Next, we adopted a two-phase estimation strategy to obtain higher quality blur kernel estimation by jointly applying kernel estimation from salient image structure and iterative support detection (ISD) kernel refinement. Finally, we used the nonblind deconvolution method based on sparse prior knowledge to restore the latent image. Extensive experiments testify to the superiority of the proposed method over state-of-the-art algorithms, both qualitatively and quantitatively. © 2016 SPIE and IS&T [DOI: 10.1117/1.JEI.25.3.033019]

Keywords: blind image deblurring; noisy and blurry image; salient structure; image edge; kernel estimation.

Paper 16138 received Feb. 26, 2016; accepted for publication May 26, 2016; published online Jun. 16, 2016.

1 Introduction

Images captured with today's cameras typically contain some degree of noise and blur. In low-light conditions, especially, blur due to motion in the scene or camera shake and noise caused by increasing camera light sensitivity with a higher ISO setting can easily ruin a photograph. The resulting information loss of visual detail both degrades scene appearance and complicates image analysis tasks. Recently, blind deblurring from a single image has been hotly discussed in the computer vision and digital image processing community for its involvement in many challenges in problem formulation, regularization, and optimization.^{1–16} Many computer vision techniques have been proposed to tackle this problem by jointly recovering a sharp latent image while estimating the blur kernel. These blind image deblurring methods generally work well when the input image has little image noise. However, their performance is impaired significantly when the image noise level increases.

For deblurring a single image, it has been demonstrated that estimating the blur kernel first and then solving a non-blind deconvolution problem with the estimated kernel renders favorable result.¹⁷ In this case, the quality of the blur kernel estimation directly affects the performance of the deblurred result. However, the high-frequency perturbations of image values caused by noise are not always ignored in deblurring techniques. When low noise assumption is not tenable, image noise may manifest itself as noise in the estimated blur kernel, which can cause the blur kernel not to be

estimated accurately. Moreover, image noise may also be amplified by deconvolution, which can lead to artifacts in the deblurred result. A possible solution is simply to apply image denoising prior to deblurring. But denoising algorithms are far from perfect, leaving behind some amount of noise while inadvertently damaging some image blur information. Therefore, estimating the blur kernel with such input also produces biased results.

To the best of our knowledge, handling noisy inputs in single image deblurring has not yet received enough attention. Although several methods^{9,11} have been proposed lately for dealing with this problem, it is still a challenge to reliably estimate the accurate blur kernel from a noisy blurred image with some complex structures.

In this paper, we propose an approach for estimating an accurate blur kernel from a noisy blurred image. Our approach still includes denoising and deblurring steps. However, we carefully design the denoising filter and deblurring procedure in a manner such that deblurring works effectively in synergy with denoising. First, we use BM3D filtering¹⁸ as a preprocess to effectively decrease the noise level in the input image. Second, we develop a method for computing image structures based on the total variation (TV) model, which is capable of excluding the edges that degrade the kernel estimation by applying image gradient selection. Third, we propose a two-phase kernel estimation method that involves kernel estimation from salient image structure and iterative support detection (ISD)¹⁹ kernel refinement, giving rise to an efficient and robust kernel estimation

*Address all correspondence to: Shijie Sun, E-mail: sunshijie@sia.cn

1017-9909/2016/\$25.00 © 2016 SPIE and IS&T

process. Finally, we employ a nonblind deconvolution method based on sparse prior knowledge to restore the latent image.

We motivate this approach with a study of how image noise degrades blur kernel estimation in blind deblurring problem. With the proposed method, we experimentally demonstrate more accurate kernel estimation and higher quality deblurring on noisy images in comparison to state-of-the-art techniques.

2 Related Work

Spatially invariant motion blur can be modeled as image convolution with a blur kernel. In this case, blind image deblurring can usually be divided into two categories: single channel blind image deblurring (SC-BID) and multiply channel blind image deblurring (MC-BID). We briefly review the SC-BID and MC-BID methods.

SC-BID aims to recover both the blur kernel and the latent image from a single blurred image. Early work usually focuses on imposing constraints on motion blur kernels and uses parameterized forms for the kernels.^{20,21} Recently, considerable progress has been made in estimating a complex motion blur kernel from a single image. The success stems partly from the employment of sparse priors and the multiscale framework. Fergus et al.¹ used a zero-mean mixture of Gaussian to fit the heavy-tailed distribution of natural image gradients. A variational Bayesian framework was employed to deblur an image. Shan et al.² exploited a unified probabilistic model for both the latent image and blur kernel. Deblurring is achieved through an alternating-minimization scheme. Cai et al.⁴ assumed that the latent images and kernels could be represented sparsely by an overcomplete dictionary and introduced a framelet and curvelet system to obtain the sparse representation for kernels and images. Levin et al.⁵ demonstrated the limitation of the common MAP methods involving estimating both the image and kernel and proposed an efficient marginal likelihood approximation.⁷ Krishnan et al.⁸ applied a normalized sparsity prior for blind kernel estimation. Sun et al.¹³ introduced a patch-based prior to estimate blur kernel. Mai and Liu¹⁶ developed a data-driven approach to fuse multiple blur kernels estimated from different existing deblurring methods into a more accurate one. A Gaussian conditional random fields-based fusion method was developed to attain the final blur kernel. Remarkably, blur kernels estimated from the aforementioned work usually contain some noise.

Another group of methods employed an explicit edge prediction step for blur kernel estimation. Especially, Joshi et al.²² predicted sharp edges by first locating step edges and then propagating the local intensity extrema toward the edge. This method was adopted to handle complex blur kernels using a multiscale scheme. Cho and Lee³ applied bilateral filtering together with shock filtering to predict sharp edges and then selected the salient edges for kernel estimation. Xu and Jia⁶ analyzed the scale of blurred edges and developed an edge selection method for robust blur kernel estimation. The kernel refinement was implemented using ISD technique. Cho et al.²³ directly detected sharp edges from blurred images and then took advantage of Radon transform to estimate the blur kernel. Pan et al.¹² further presented an effective mask computation algorithm to adaptively select useful edges for kernel estimation. Zhou

and Komodakis²⁴ imposed a geometric parsing prior on general MAP-estimation framework for blind image deblurring. Although the performance of these methods has improved impressively, the estimated kernels still embrace some noise occasionally, the sparsity of which also cannot be guaranteed.

MC-BID tries to combine complementary information from multiple images for generating higher quality image estimates, in comparison with SC-BID. Chen et al.²⁵ presented a dual-image deblurring method to restore a sharp image from two consecutively captured blurred photos with different blur kernels. Zhuo et al.²⁶ exploited the correlation between sharp images and their corresponding flash images and then used a pair of blurred and flash images to produce a sharp one. Interested readers can refer to Refs. 27,28 for more details.

While there have been significant advances in blind image deblurring, the abovementioned methods all presume very little noise in the input image. The hypothesis is not always realistic for real-world images. When the noise level increases, the estimated blur kernel becomes noisy and results in greater error in the deconvolution process. To suppress noise, Tai and Lin⁹ used an existing denoising package as a preprocess and then estimated the blur kernel and the latent image from the denoised result. Zhong et al.¹¹ showed that directly applying image denoising methods partially damaged the blur information, leading to biased kernel estimation and then used directional filters together with Radon transform to estimate the blur kernel from a noisy blurred image. It is notable that these methods are not always able to produce accurate blur kernel estimations and reconstruct sharp latent images.

3 Effects of Image Noise in Blur Kernel Estimation

In this section, we analyze the effect of image noise in blur kernel estimation. For simplicity, we assume that the blur kernel is spatially invariant. The formation process of image blur is generally modeled as

$$b = l * k + n, \quad (1)$$

where b is the observed noisy and blurry image, l is the latent image, k is the blur kernel or the point-spread-function, n is some additive noise introduced during image acquisition, and “ $*$ ” is the convolution operator. In blind image deblurring, estimating both k and l from b is a well-known ill-posed inverse problem, and the additional noise n makes this problem even more challenging. To simplify things, previous SC-BID methods usually assume the input image b to be nearly noise-free. However, the noise in the real-world blurred images cannot always be negligible.

For the sake of the convenience of analysis, the Fourier transform of Eq. (1) in the frequency domain can be expressed as

$$B = KL + N, \quad (2)$$

where B , L , K , and N denote the Fourier transform of b , l , k , and n , respectively. Our analysis is carried on using the alternating-optimization framework for blind image deblurring. Let L^{i-1} be the latent image of the $(i-1)$ 'th iteration in the frequency domain. If image noise is nearly negligible, the blur kernel K^i at the i 'th iteration can be computed in the frequency domain from Eq. (2) as $K^i = (B/L^{i-1})$.

However, when image noise becomes nonsignificant, dividing the input image by the estimated latent image leads to

$$K^i = \frac{B'}{L^{i-1}} + \frac{N}{L^{i-1}}, \quad (3)$$

where B' represents the ideal blurred image without noise. From Eq. (3), we can discover that the estimated blur kernel is offset by the term N/L^{i-1} , and the image noise is transferred into the estimated blur kernel. When the amount of image noise increases, clearly the noise level in K^i also increases and, hence, the error between the estimated blur kernel and the ground truth kernel becomes greater (Fig. 1).

4 Our Approach

4.1 Process Overview

Figure 2 shows the overall process of our SI-BID method, which builds upon the coarse-to-fine, iterative optimization framework commonly adopted in recent methods. To progressively refine the blur kernel from a noisy and blurred input image, our method contains three key steps: denoising, kernel initialization, and kernel refinement. In the first step, we apply BM3D filtering as a preprocess to effectively decrease the noise level of the input image, which can help to extract more reliable image structures or edges for blur kernel estimation. In the second step, we extract the main image structures from the input of the denoising step, then use shock filter to restore strong edges from the extracted structures and select some salient edges with large pixel values for estimating the kernel initialization. The whole kernel initialization process is performed in a coarse-to-fine, multiscale iterative optimization manner (the dashed blue box in Fig. 2). In the final step, we apply an ISD method to refine the kernel estimation of the previous step while removing noise.

In the coarse-to-fine iterative process for updating the blur kernel and the latent image, we use the grayscale versions of the denoised input and the latent image. After the final blur kernel has been estimated at the finest level (i.e., the latent

image is the same size as the input image), we perform the final deconvolution with the estimated kernel on each color channel of the denoised image to obtain the deblurred result.

4.2 Denoising as a Preprocess

From the analysis in the previous section, we observe that kernel estimation is very sensitive to image noise. In the condition that input images contain non-negligible noise, many previous SI-BID methods cannot produce the reliable blur kernel estimation from a noisy blurred image.¹¹ In general, motion blurring and image noising are considered to be two independent processes in image formation. To a certain extent, using denoising preprocessing to suppress the noise in the input image can ameliorate the problem of the noise in kernel estimation. Although this can inevitably lead to over-smoothing of image details and loss of blurry information, inaccuracy blur kernels can be estimated effectively. Therefore, denoising the input image before applying the blind image deblurring process can partly help to improve the performance of the previous approaches. To better understand the effect of image denoising on the blur kernel estimation, we conduct an experiment, shown in Fig. 3. In this experiment, we apply BM3D to a real-world noisy and blurry test image and then use Xu and Jia's method⁶ and Pan and Liu's method¹² to estimate the blur kernel and restore the latent image, respectively. The experimental results of Refs. 6, 12 are all generated by using the authors' source code or executable program downloaded online.

Figures 3(b) and 3(c) show that the performance of Xu and Jia's method is improved using denoising as a preprocess. However, Figs. 3(d) and 3(e) show that image denoising is not able to ensure Pan and Liu's method, compared with Xu and Jia's method, to obtain the satisfied result. This indicates that directly denoising the noisy and blurred image before applying the existing blind image deblurring methods cannot lead to a reliable result. The main reason is that sophisticated denoising algorithms remove not only a large amount of noise but also some image structure. Deblurring with such input can lead to undesirable results, such as inaccuracy blur kernel estimation, edge artifacts, and loss of image structure.

4.3 Two-Stage Blur Kernel Estimation

4.3.1 Kernel initialization from salient structure

In the kernel initialization, we aim to compute a coarse version of the blur kernel in a multiscale setting. Kernel estimation based on salient structure contains three main steps, i.e., reliable structure extracting, kernel estimation, and coarse image restoration.

Reliable structure extracting. Adaptively selecting salient image edges can be achieved using the structure-texture decomposition method. For an image l with intensity value $l(x)$ at pixel x , the structure component l_{src} can be obtained by minimizing the following objective function:¹²

$$l_{\text{src}} = \arg \min_{l_{\text{src}}} \|\nabla l_{\text{src}}\|_2 + \frac{1}{2\theta\omega(x)} \|l_{\text{src}} - l\|_2^2, \quad (4)$$

where θ is an adjustable parameter, $\omega(x) = \exp(-\|r(x)\|^{0.8})$ and $r(x)$ is a metric to measure the usefulness of image gradients and defined as



Fig. 1 Image noise influence in blur kernel estimation. (a) The input blurred image and the ground truth blur kernel (overlaid). (b) Blur kernels estimated using the method of Xu and Jia⁶ under increasing noise levels, from 0% to 40%. When the noise level of the input image increases, the estimated blur kernels degrade seriously.

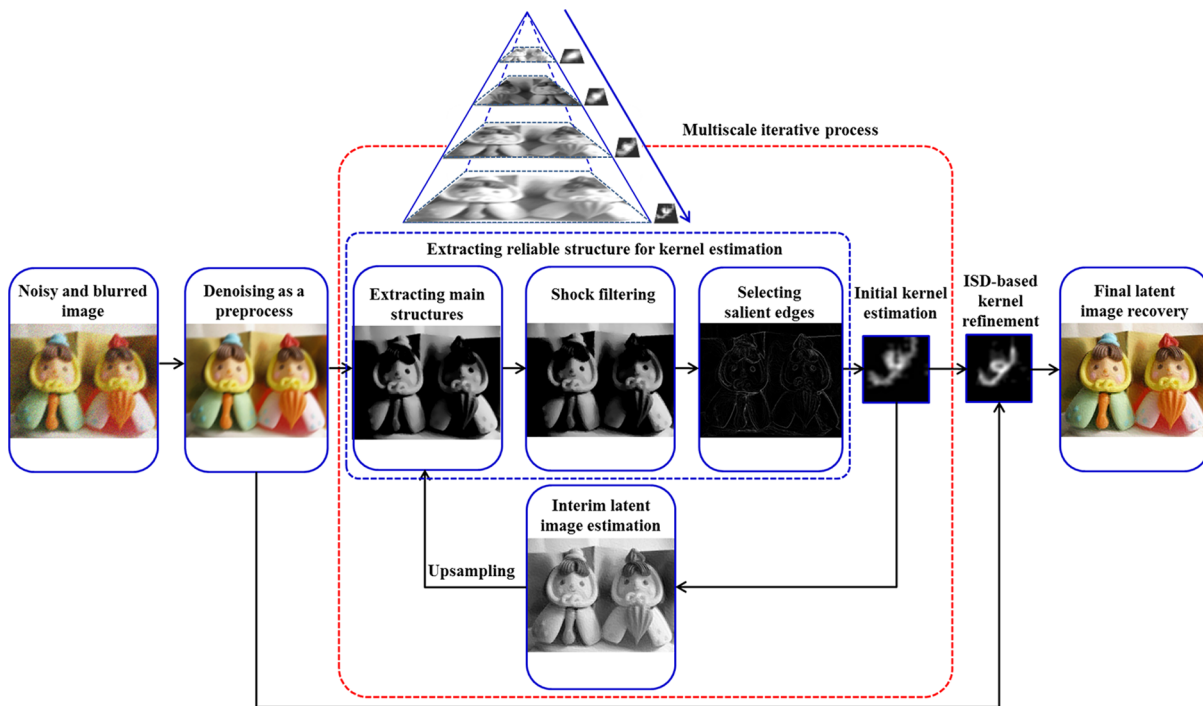


Fig. 2 Overview of our SI-BID process. The red dotted line box encloses the process of iterative kernel estimation.

$$r(x) = \frac{\|\sum_{y \in N_h(x)} \nabla b(y)\|_2}{\sum_{y \in N_h(x)} \|\nabla b(y)\|_2 + 0.5}, \quad (5)$$

in which b is the noisy and blurred image and $N_h(x)$ is an $h \times h$ window centered at pixel x . This equation is first used

in Ref. 10 to remove some narrow strips that may be averse to kernel estimation. A smaller r implies that the local region is either flat or includes some spikes, whereas larger r indicates that local window contains strong image structures. The adoptive weight $\omega(x)$ has the similar advantages to the metric r , having a strong penalty to those areas that are flat or contain narrow strips as well. Furthermore, the

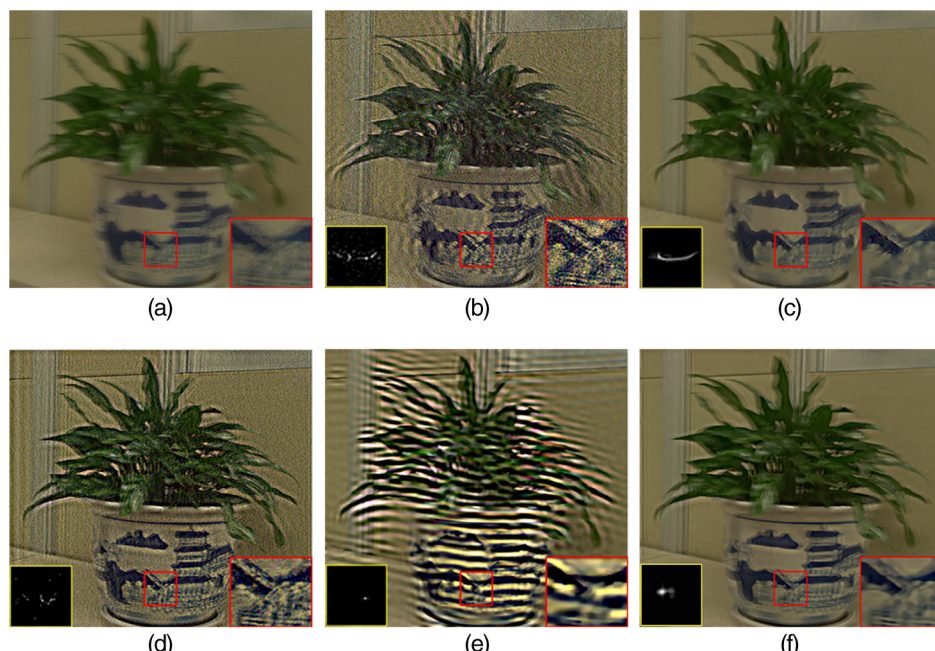


Fig. 3 Comparison on a real-world example. (a) Noisy and blurry image. (b) Result from Xu and Jia. (c) Result from Xu and Jia with denoising as a preprocess. (d) Result from Pan and Liu. (e) Result from Pan and Liu with denoising as a preprocess. (f) Our result. Estimated blur kernel (size: 41 × 41) and a zoom-in region are also shown.

stair-casing effect that Eq. (4) may introduce can be mitigated effectively by adjusting the value of θ to be large in the smooth areas and small near the edges.

After computing \tilde{l}_{src} , we solve the following shock filtering PDE problem to construct the enhanced structure $\tilde{l}_{\text{src}}^{29}$:

$$\begin{cases} \partial \tilde{l}_{\text{src}} / \partial t = -\text{sign}(\Delta \tilde{l}_{\text{src}}) \|\nabla \tilde{l}_{\text{src}}\|_2, \\ \tilde{l}_{\text{src}}|_{t=0} = l_{\text{src}}, \end{cases} \quad (6)$$

where $\nabla \tilde{l}_{\text{src}}$ and $\Delta \tilde{l}_{\text{src}}$ are the first- and second-order spatial derivatives of \tilde{l}_{src} , respectively.

Finally, the salient edges used for kernel estimation can be determined as

$$\nabla S = \nabla \tilde{l}_{\text{src}} \circ H(M, \tau), \quad (7)$$

where “ \circ ” denotes the pixelwise multiplication operator, $H(M, \tau)$ is the unit binary mask function and defined as

$$H(M, \tau) = \begin{cases} 1, & M_{x,y} \geq \tau, \\ 0, & M_{x,y} < \tau, \end{cases} \quad (8)$$

in which $M = \|\nabla \tilde{l}_{\text{src}}\|_2$ and $M_{x,y}$ denote the magnitude of the gradient of \tilde{l}_{src} at coordinates (x, y) , and τ is a threshold of the gradient magnitude. Here, we determine the initial value of τ according to the method of Ref. 3 at the beginning of the iterative deblurring process. Specifically, the directions of image gradient are initially quantized into four groups. τ is set to guarantee that at least $0.5\sqrt{N_l N_k}$ pixels participate in blur kernel estimation in each group, where N_l and N_k are the total number of pixels in the input image and the kernel, respectively.

Initial kernel estimation. Most work assumes that the distributions of blur kernels can be modeled by Hyper-Laplacian, which can preserve the sparsity of blur kernels but not ensure the continuity. To preserve the continuity of estimated blur kernels, we introduce the image smoothing method based on L_0 gradient minimization³⁰ to handle the estimated kernels. Initial kernel estimation can be accomplished by minimizing the objective function defined as

$$k = \arg \min_k \|\nabla b - \nabla S * k\|_2^2 + \gamma \|k\|_\alpha^\alpha + \mu C(k), \quad (9)$$

where γ and μ are the weights that control the sparsity and smoothness of k , respectively, $0 < \alpha \leq 1$ and $C(k) = \{(x, y) | |\partial_x k(x, y)| + |\partial_y k(x, y)| \neq 0\}$ (i.e., $C(k)$ counts the number of pixels, the magnitudes of whose gradients are not zeros).

Equation (9) is difficult to be minimized directly as it is a nonconvex optimization problem. For this reason, we can employ an efficient alternating-minimization method to resolve it. Equation (9) can be written equivalently as

$$\begin{cases} k = \arg \min_k \|\nabla b - \nabla S * k\|_2^2 + \gamma \|k\|_\alpha^\alpha \\ k = \arg \min_k \|\hat{k} - k\|_2^2 + \mu C(k) \end{cases}. \quad (10)$$

Algorithm 1. Kernel initialization from salient structure

Input: Blur image b_0 (b_0 is the denoised version of the input image b) and an all-zero kernel (size: $h \times w$)

Determine the number of image pyramid m according to the size of kernel.

for $i = 1$ to m **do**

 Downsample b_0 to get b_0^i according to the current image pyramid.

for $j = 1$ to n (n is the number of iterations) **do**

 (a) Select salient edges ∇S for kernel estimation according to Eq. (7).

 (b) Estimate blur kernel k according to Eq. (10).

 (c) Estimate the latent image I^i according to Eq. (11), and update

$\tau \leftarrow \tau / 1.1$, $\theta \leftarrow \theta / 1.1$.

end for

 Upsample image $I^{i+1} \leftarrow I^i \uparrow$

end for

Output: Blur kernel k^0 and sharp salient edge gradient map ∇S .

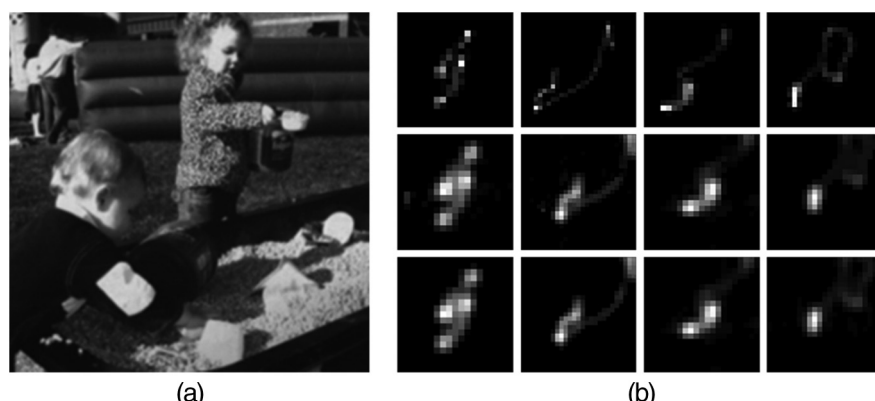


Fig. 4 Comparison of results with and without the constraint $C(k)$. (a) The ground truth image. (b) Kernels. The top row shows the real-world kernels, the middle row shows the kernel estimations without the constraint, and the bottom row shows the kernel estimations with the constraint.

For Eq. (10), the first objective function can be resolved by the constrained iterative reweighted least square (IRLS) method,³¹ and the second objective function can be optimized by using the alternating-optimization method in Ref. 30. We empirically set $\alpha = 0.5$, $\gamma = 0.01$, and $\mu = 10^{-3}$ to 10^{-5} .

To demonstrate the effectiveness of the constraint $C(k)$ in the kernel estimation process, we choose the test set provided by Ref. 5 to conduct an experiment shown in Fig. 4. From Fig. 4(b), the kernel estimations with the constraint outperform those without adopting the constraint, which demonstrates that the continuity and accuracy of kernel estimate with the constraint have been greatly improved. Here, although introducing the continuity constraint in the kernel estimation does increase computational loads to some extent, it can improve the accuracy and continuity of kernel estimation in each image level (our initial kernel estimation is based on multiscale framework), which avoids degrading the intermediate blur kernel quality.

Coarse image restoration. For this deconvolution stage, the main purpose is to restore the sharp edges from the blurred image. Hence we use an anisotropic TV model to guide the recovery of a coarse version of the latent image. The objective function is

Algorithm 2. ISD-based blur kernel refinement algorithm

Input: Blur image b_0 (b_0 is the denoised version of the input image b), initial kernel k^0 , and salient structure ∇S (output from Algorithm 1.)

Compute the initial set \overline{S}^0 on kernel k^0 according to Eq. (12).

repeat

(a) Estimate blur kernel k^i according to Eq. (13).

(b) Update \overline{S}^i according to Eq. (12).

(c) $i \leftarrow i + 1$

until $\|k^{i+1} - k^i\|/\|k^i\| \leq \epsilon^s$ ($\epsilon^s = 1e^{-3}$ empirically) or the maximum iteration limit is reached (here set i to 3).

Output: Blur kernel k^s .

$$l = \arg \min_l \|b - l * k\|_2^2 + \lambda_l \|\nabla l\|_1, \quad (11)$$

where the parameter λ_l is a regularization weight and empirically set to 0.1. We employ the IRLS method to obtain the solution of Eq. (11). When the solver iterates among solving l , we empirically run two iterations in outer IRLS system and use 100 conjugate gradient iterations in the inner IRLS system.

To obtain a better reasonable kernel estimation, we also apply multiscale estimation of the kernel using a coarse-to-fine pyramid of image resolutions, which is similar to that in Ref. 2. During building the pyramid, the downsampling factor is set to $1/\sqrt{2}$. Similar to the strategy of Ref. 12, the number of pyramid levels is adaptively determined by the size of blur kernel, so the blur kernel at the coarsest level has a width or height of around 3 to 7 pixels. As the iteration goes, we gradually decrease the values of θ and τ by dividing 1.1 at each pass, to include more and more edges for kernel estimation. The details of our initial kernel estimation are shown in Algorithm 1.

4.3.2 Iterative support detection-based kernel refinement

ISD¹⁹ is a sparse signal reconstruction method that can achieve fast reconstruction while requiring very few measurements. It is first applied by Ref. 6 to correct imperfect kernel estimates. To obtain more accurate kernel estimations, we use the ISD method to improve the initial kernel quality that may possibly be degraded due to image denoising. ISD is an iterative framework. At the beginning of each iteration, large-value elements of previously estimated kernel k^i are put into a set S^{i+1} and others belong to the set S^{i+1} . S^{i+1} is constructed as

$$\overline{S}^{i+1} \leftarrow \{j : k_j^i \leq \epsilon^s\}, \quad (12)$$

where the parameter j indexes the elements in k^i and ϵ^s is a positive number and can be determined by using the “first significant jump” rule. For a $h \times w$ blur kernel, ϵ^s is empirically configured as, where $\epsilon^s = 7 \times \|k^i\|_\infty / (2h \times w \times N_{\text{iter}})$ returns the largest value in k^i and N_{iter} is the number of iteration. Then we minimize

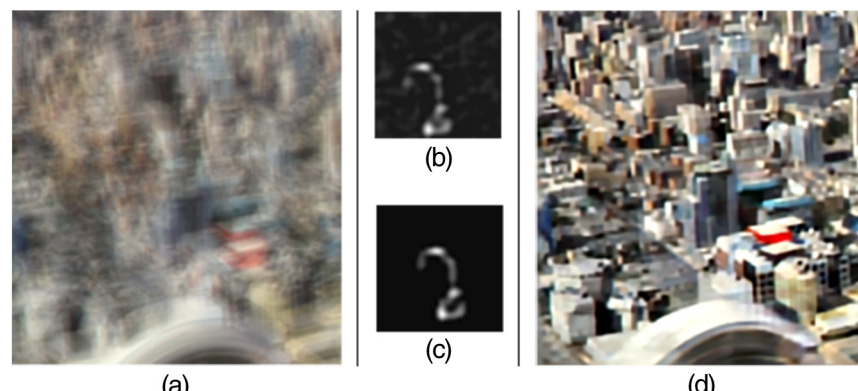


Fig. 5 An example of kernel refinement. (a) A blurred image. (b) Initial kernel estimation. (c) Refined kernel using ISD-based method. (d) Restored image using the refined kernel.

$$k = \arg \min_k \frac{1}{2} \|\nabla S * k - \nabla b\|_2^2 + \gamma' \sum_{j \in S^{i+1}} |k_j| \quad (13)$$

for blur kernel refinement. In Eq. (13), ∇S and k are the salient structure and blur kernel, respectively, that are outputted from Algorithm 1. Equation (13) is a classical truncated

L_1 minimization problem and can be resolved via IRLS method. Our whole kernel refinement algorithm is summarized in Algorithm 2.

An example of kernel refinement is shown in Fig. 5. We adopt a blurred image with rich edge information from Ref. 6 as the blurred input [shown in Fig. 5(a)]. From Figs. 5(b) and

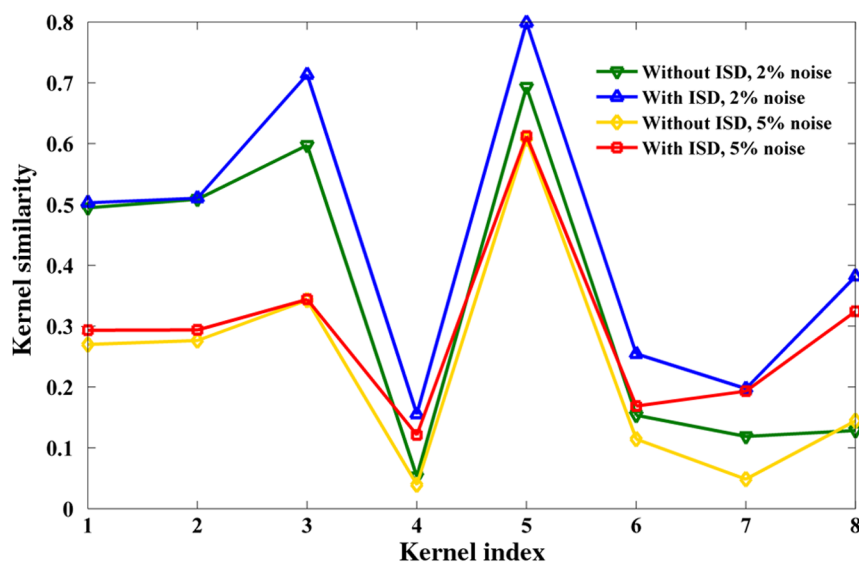


Fig. 6 Comparison of kernel similarity with and without ISD refinement.



Fig. 7 The dataset of Ref. 5. (a) Sharp images and (b) real-world kernels.

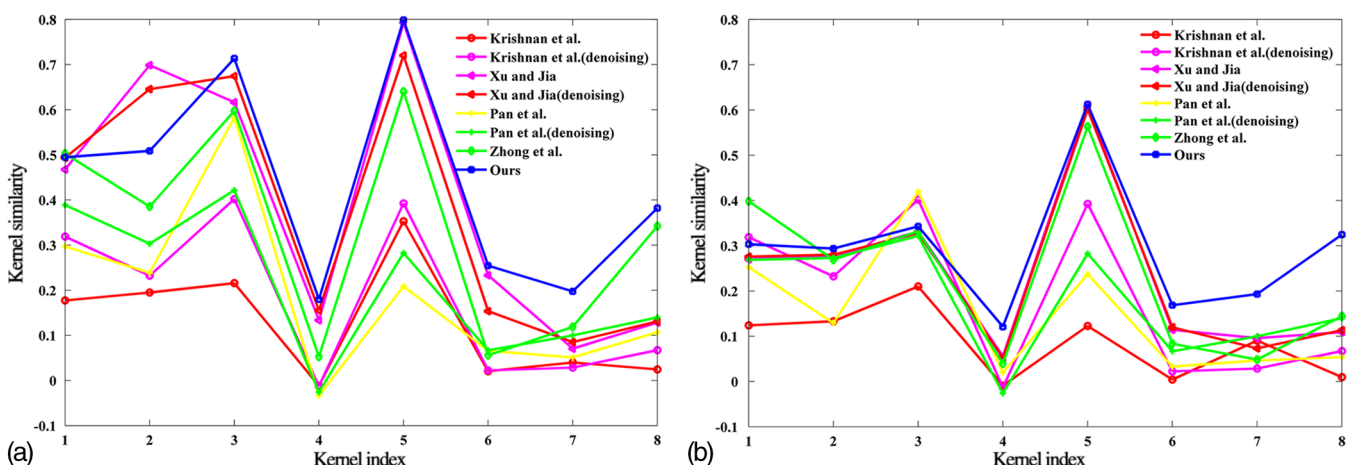


Fig. 8 Performance comparison using the kernel similarity with state-of-the-art methods on the synthetic dataset. Overall, our method performs the best. (a) Test with 2% additive Gaussian noise. (b) Test with 5% additive Gaussian noise.

Table 1 Quantitative comparison on the synthetic dataset.

Image	Methods	PSNR		SSIM	
		2% noise	5% noise	2% noise	5% noise
Image 1	Krishnan et al.	18.9024	16.8873	0.3177	0.1824
	Krishnan et al. (denoising)	20.9868	16.4301	0.6285	0.4321
	Xu and Jia	18.8434	9.7462	0.3429	0.0848
	Xu and Jia (denoising)	23.5335	19.4620	0.7319	0.5233
	Pan et al.	21.9983	12.9521	0.5247	0.1449
	Pan et al. (denoising)	22.4054	17.8629	0.6925	0.5387
	Zhong et al.	22.4829	21.9534	0.6697	0.5279
	Ours	25.6226	23.6871	0.8013	0.6741
Image 2	Krishnan et al.	19.8945	18.0731	0.3058	0.1879
	Krishnan et al. (denoising)	18.4236	15.6033	0.4969	0.3270
	Xu and Jia	19.2374	9.7663	0.3733	0.0807
	Xu and Jia (denoising)	21.5423	17.3280	0.5692	0.3352
	Pan et al.	20.7609	12.9928	0.4466	0.1232
	Pan et al. (denoising)	18.7072	15.5467	0.5339	0.3981
	Zhong et al.	23.1148	21.3014	0.6419	0.4277
	Ours	24.8491	23.1060	0.7435	0.6338
Image 3	Krishnan et al.	19.7009	17.8211	0.3491	0.2155
	Krishnan et al. (denoising)	16.2360	14.5125	0.5952	0.4013
	Xu and Jia	18.8854	9.9347	0.3513	0.0981
	Xu and Jia (denoising)	25.0746	21.9823	0.7908	0.6390
	Pan et al.	21.3722	12.3951	0.5221	0.1485
	Pan et al. (denoising)	16.1595	14.7548	0.6156	0.4931
	Zhong et al.	21.1571	20.9218	0.5984	0.4526
	Ours	25.8938	22.7557	0.8281	0.6359

Table 1 (Continued).

Image	Methods	PSNR		SSIM	
		2% noise	5% noise	2% noise	5% noise
Image 4	Krishnan et al.	19.1952	17.1793	0.3053	0.1695
	Krishnan et al. (denoising)	14.4661	14.1269	0.5504	0.4125
	Xu and Jia	17.0998	9.3686	0.2435	0.0449
	Xu and Jia (denoising)	23.0323	20.7000	0.6582	0.5239
	Pan et al.	20.9163	12.2293	0.4213	0.0901
	Pan et al. (denoising)	13.6531	15.2382	0.5348	0.4635
	Zhong et al.	22.8173	22.0987	0.6656	0.5335
	Ours	23.4714	22.8390	0.6817	0.5355

5(c), the final result after kernel refinement apparently preserves the continuity of kernel while efficiently removing noise in the initial kernel. To further demonstrate the effectiveness of ISD-based kernel refinement method, we test this algorithm on the synthetic 64-image test set, which is established by adding 2% and 5% additive Gaussian noise to widely used blurred images introduced in Ref. 5. The similarity measured between the estimated kernels and the ground truth is employed to compare the estimation accuracy for the blur kernels in Fig. 6. One can see that the accuracy of kernel estimation after ISD-based kernel refinement has been improved effectively.

4.4 Final Image Restoration

Once an accurate kernel k^s is estimated, we can use it to recover a good latent image l by using many nonblind deconvolution methods. Here a Hyper-Laplacian prior with $L_{0.8}$ -norm regularization is employed. Our final objective function for latent image restoration is defined as

$$l = \arg \min_l \|b_0 - l * k\|_2^2 + \lambda \|\nabla l\|_\alpha^\alpha, \quad (14)$$

where b_0 is the denoised version of the noisy and blurred input b , $\nabla l = (\partial_x l, \partial_y l)$ and $\alpha = 0.8$. Equation (14) can also be efficiently resolved by the IRLS method.

It is noted that the previous methods utilized the original noisy blurred image to select the raw information for kernel estimation in different ways, which helped to refine the blur kernel estimation. In comparison, our method makes full use of the valuable edge information of the denoised input image to estimate the initial blur kernel and then adopts the ISD method to refine the initial blur kernel estimation. Moreover, in the final image restoration, we adopt not the original input image but the denoised version of it as the blurred observation to conduct nonblind deconvolution. This is mainly because image noise will be amplified in nonblind deconvolution. To overcome this problem, we have to strike a balance between denoising and oversmoothing, as do the previous

methods (e.g., Ref. 9 applied the denoising operation at the beginning of each iteration, and Ref. 11 introduced the non-local means filter in nonblind deconvolution step).

5 Experimental Results

We first tested our algorithm on the widely used image test set introduced in Ref. 5 and further conducted experiments on the real-world images provided in Ref. 9. Then we compared our results with those of the state-of-the-art methods.^{6,8,9,11,12}

For all the experiments, some implementation details are as follow. In the denoising process, we experimentally set the standard deviation σ for BM3D filtering to 15 according to many experiments and adopt default values for other parameters. In the kernel estimation, all color images are converted to grayscale ones. The initial value of θ in Eq. (4) is set to 1, the size of local window $N_h(x)$ in Eq. (5) is set to 11×11 , α , γ , and μ in Eq. (10) are set to 0.5, 0.01, and 10^{-3} to 10^{-5} , respectively; λ_i in Eq. (11) is set to 0.005, γ' in Eq. (13) is set to 0.01, and λ in Eq. (14) is set to 0.003. In the final latent image estimation, each color channel is processed separately. We implemented our method in MATLAB® on a PC running MS Windows 8 64 bit version with Intel Core i5 CPU 2.20 GHz and 8 GB RAM.

We make use of three measurements for quantitative analysis: kernel similarity introduced in Ref. 10, and mean peak signal-to-noise ratio (PSNR) and mean structural similarity (SSIM) employed in Ref. 32.

5.1 Quantitative Evaluation on the Synthetic Test Dataset

The synthetic dataset in Ref. 5 contains 32 test images produced from four sharp grayscale images of size 255×255 and eight real-world motion blur kernels, as shown in Fig. 7 and available online.⁵ Based on this dataset, we added 2% and 5% additive Gaussian noise by using Photoshop to simulate the effects of camera noise, producing two test sets with different noise level. The kernel similarity between the estimated kernels and the ground truth using the maximum correlation in Ref. 10 is used to measure the quality of the estimated results. We compare our method with those of Xu and Jia⁶, Krishnan et al.,⁸ Zhong et al.,¹¹ and Pan et al.¹² Figure 8 shows the kernel similarity performance, which suggests that, overall, our method outperforms other competing methods on the two test sets. We also employ mean PSNR³³ and mean SSIM^{13,32} to quantitatively evaluate the estimation accuracy for the restored image. The results are shown in Table 1. Our method provides both higher mean PSNR value and higher mean SSIM value.

Additionally, we also compare the processing time for the deblurring examples in Fig. 8, as shown in Table 2. Here the processing time includes the time for the final nonblind deconvolution. From Table 2, our MATLAB® implementation spends about 2 min to deblur a 255×255 gray image with a 27×27 kernel in our test environment. Compared with other techniques, our method needs more computational time due to involving both denoising step and nonconvex optimization in kernel estimation. However, we believe that our method is able to run faster by using its C++ implementation with GPU acceleration.

Table 2 Time of the deblurring examples in Fig. 8.

Size		Methods	Processing time (s)
Image	Kernel		
255×255	19×19	Krishnan et al.	61.8504
		Krishnan et al. (denoising)	65.1460
		Xu and Jia	132.0575
		Xu and Jia(denoising)	135.3531
		Pan et al.	106.2172
		Pan et al. (denoising)	109.5128
		Zhong et al.	75.6749
255×255	21×21	Ours	112.5069
		Krishnan et al.	104.7758
		Krishnan et al. (denoising)	108.0488
		Xu and Jia	64.3586
		Xu and Jia (denoising)	67.6316
		Pan et al.	105.6167
		Pan et al. (denoising)	107.8793
255×255	27×27	Zhong et al.	82.2884
		Ours	110.9770
		Krishnan et al.	102.0768
		Krishnan et al. (denoising)	105.3769
		Xu and Jia	94.6199
		Xu and Jia (denoising)	97.92
		Pan et al.	118.5252
255×255	23×23	Pan et al. (denoising)	121.8253
		Zhong et al.	84.8104
		Ours	125.4384
		Krishnan et al.	97.6505
		Krishnan et al. (denoising)	100.9131
		Xu and Jia	64.4539
		Xu and Jia (denoising)	67.7165
255×255	21×21	Pan et al.	107.6167
		Pan et al. (denoising)	110.8793
		Zhong et al.	81.0989
		Ours	114.1294



Fig. 9 A real-world image with unknown camera shake. (a) Input noisy and blurry image. (b) Result from Krishnan et al. (c) Result from Xu and Jia. (d) Result from Pan et al. (e) Result from Tai and Lin. (f) Result from Zhong et al. (g) Our result. The estimated blur kernel and zoom-in regions are also shown. Our result contains more high-frequency details and fewer ringing artifacts.

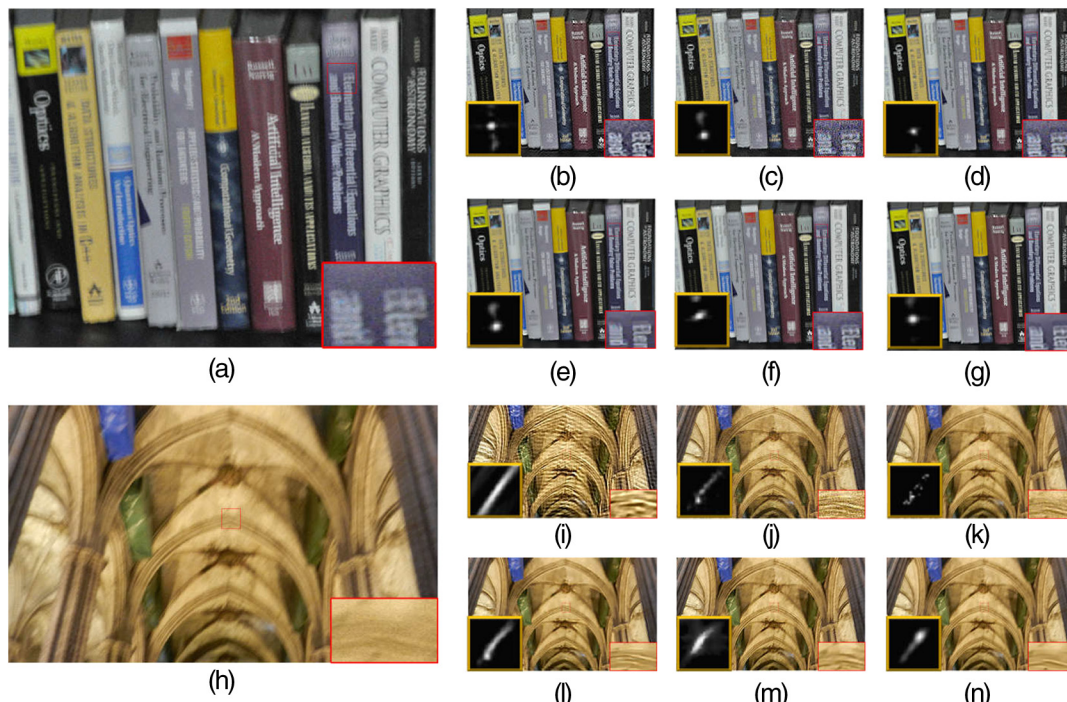


Fig. 10 Another real-world images with unknown camera shake. (a) and (h) Input noisy and blurry images, (b) and (i) results from Krishnan et al., (c) and (j) results from Xu and Jia, (d) and (k) results from Pan et al., (e) and (l) results from Tai and Lin, (f) and (m) results from Zhong et al., (g) and (n) our results. Our method produces competitive results.

5.2 Evaluation on Real Noisy and Blurred Images

The test images in Ref. 5 are only 255×255 in size and limited in terms of diversity. In order to further demonstrate the effectiveness of our method, we conducted experiments on real noisy and blurred images of low-light scenes, which were captured using a Nikon D90 DSLR camera with a high ISO setting and long-exposure period in Ref. 9. Then we compare our results with those of other state-of-the-art methods, including Xu and Jia⁶, Krishnan et al.,⁸ Tai and Lin,⁹ Zhong et al.,¹¹ and Pan et al.¹² The results are shown in Figs. 9 and 10. One can see that our algorithm outperforms these methods run with optimum parameters for deblurring. Furthermore, our recovered latent images exhibit fewer artifacts and contain more high-frequency details at the same time.

6 Conclusion

We have shown that most state-of-the-art image deblurring methods are very sensitive to image noise. In this paper, we propose a new kernel estimation method based on image salient edges. We discovered that directly denoising noisy and blurred images before applying the previous deblurring techniques cannot lead to reliable results. Therefore, we combine effective denoising with kernel estimation using image salient edges and ISD-based kernel refinement together to handle noise in single image deblurring. Compared with the previous methods, our method produces more accurate kernel estimations and better deblurred results. The effectiveness of the proposed approach is demonstrated in several comparisons on synthetic and real data.

Acknowledgments

This work was in part supported by the General Scientific Research Project of Education Department of Liaoning of China under Grant No. L2015368. We would like to thank Dr. Yu-Wing Tai at the Korea Advanced Institute of Science and Technology for sharing his images. Shijie Sun would like to thank Dr. Jinshan Pan at UC Merced for providing his MATLAB® program.

References

- R. Fergus et al., "Removing camera shake from a single photograph," *ACM Trans. Graph.* **25**(3), 787–794 (2006).
- Q. Shan, J. J. Jia, and A. Agarwala, "High-quality motion deblurring from a single image," *ACM Trans. Graph.* **27**(3), 15–19 (2008).
- S. Cho and S. Lee, "Fast motion deblurring," *ACM Trans. Graph.* **28**(5), 145 (2009).
- J. F. Cai et al., "Blind motion deblurring from a single image using sparse approximation," in *Proc. IEEE Computer Society Conf. on Computer Vision and Pattern Recognition*, pp. 104–111, IEEE, Miami Beach, Florida (2009).
- A. Levin et al., "Understanding and evaluating blind deconvolution algorithms," in *Proc. IEEE Computer Society Conf. on Computer Vision and Pattern Recognition*, pp. 1964–1971, IEEE, Miami Beach, Florida, 2009, <http://www.wisdom.weizmann.ac.il/~levina/papers/LevinEtalCVPR09Data.rar>.
- L. Xu and J. Y. Jia, "Two-phase kernel estimation for robust motion deblurring," in *Proc. of European Conf. on Computer Vision*, pp. 157–170, Heraklion, Greece, 2010, <http://www.cse.cuhk.edu.hk/~leojia/programs/RobustMotionDeblur.zip>.
- A. Levin et al., "Efficient marginal likelihood optimization in blind deconvolution," in *Proc. IEEE Computer Society Conf. on Computer Vision and Pattern Recognition*, pp. 2657–2664, IEEE, Colorado, Springs (2011).
- D. Krishnan, T. Tay, and R. Fergus, "Blind deconvolution using a normalized sparsity measure," in *Proc. IEEE Computer Society Conf. on Computer Vision and Pattern Recognition*, pp. 233–240, IEEE, Colorado, Springs (2011).
- Y. W. Tai and S. Lin, "Motion-aware noise filtering for deblurring of noisy and blurry images," in *Proc. IEEE Computer Society Conf. on Computer Vision and Pattern Recognition*, pp. 17–24, IEEE, Providence, Rhode Island (2012).
- L. Xu, S. Zheng, and J. Y. Jia, "Unnatural L_0 sparse representation for natural image deblurring," in *Proc. IEEE Computer Society Conf. on Computer Vision and Pattern Recognition*, pp. 1107–1114, IEEE, Portland, Oregon (2013).
- L. Zhong et al., "Handling noise in single image deblurring using directional filters," in *Proc. IEEE Computer Society Conf. on Computer Vision and Pattern Recognition*, pp. 612–619, IEEE, Portland, Oregon (2013).
- J. S. Pan et al., "Kernel estimation from salient structure for robust motion deblurring," *Signal Process. Image Commun.* **28**(9), 1156–1170 (2013) https://www.dropbox.com/seixia2nsg15mhk/Deblurring_code_v2.zip.
- L. B. Sun et al., "Edge-based blur kernel estimation using patch priors," in *Proc. of IEEE Int. Conf. on Computational Photography*, pp. 1–8, 19–21, IEEE, Cambridge, Massachusetts (2013).
- T. Michaeli and M. Irani, "Blind deblurring using internal patch recurrence," in *Proc. of European Conf. on Computer Vision*, pp. 783–798, Zurich, Switzerland (2014).
- X. C. Cao et al., "Scene text deblurring using text-specific multiscale dictionaries," *IEEE Trans. Image Process.* **24**(4), 1302–1314 (2015).
- L. Mai and F. Liu, "Kernel fusion for better image deblurring," in *Proc. IEEE Computer Society Conf. on Computer Vision and Pattern Recognition*, pp. 371–380, Boston, Massachusetts (2015).
- Z. Hu and M. H. Yang, "Good regions to deblur," in *Proc. of European Conf. on Computer Vision*, pp. 59–72, Florence, Italy (2012).
- K. Dabok, A. Danieyan, and A. Foi, "Image and video denoising by sparse 3D transform-domain collaborative filtering," <http://www.cs.tut.fi/~foi/GCF-BM3D> (2014).
- Y. Wang and W. Yin, "Sparse signal reconstruction via iterative support detection," *SIAM J. Imaging Sci.* **3**(3), 462–491 (2010).
- T. F. Chan and C. K. Wong, "Total variation blind deconvolution," *IEEE Trans. Image Process.* **7**(3), 370–375 (1998).
- Y. L. You and M. Kaveh, "Blind image restoration by anisotropic regularization," *IEEE Trans. Image Process.* **8**(3), 396–407 (1999).
- N. Joshi, R. Szeliski, and D. J. Kriegman, "PSF estimation using sharp edge prediction," in *Proc. IEEE Computer Society Conf. on Computer Vision and Pattern Recognition*, pp. 3823–3830, Anchorage, Alaska (2008).
- T. S. Cho et al., "Blur kernel estimation using the Radon transform," in *Proc. IEEE Computer Society Conf. on Computer Vision and Pattern Recognition*, pp. 241–248, IEEE, Colorado, Springs (2011).
- Y. P. Zhou and N. Komodakis, "A MAP-estimation framework for blind deblurring using high-level edge priors," in *Proc. of European Conf. on Computer Vision*, pp. 142–157, Zurich, Switzerland (2014).
- J. Chen et al., "Robust dual motion deblurring," in *Proc. IEEE Computer Society Conf. on Computer Vision and Pattern Recognition*, pp. 3791–3798, IEEE, Anchorage, Alaska (2008).
- S. J. Zhuo, D. Guo, and T. Sim, "Robust flash deblurring," in *Proc. IEEE Computer Society Conf. on Computer Vision and Pattern Recognition*, pp. 2440–2447, IEEE, San Francisco, California (2010).
- W. Li, J. Zhang, and Q. H. Dai, "Robust blind motion deblurring using near-infrared flash image," *J. Vis. Commun. Image Represent.* **24**(8), 1394–1413 (2013).
- H. S. Li et al., "Joint motion deblurring with blurred/noisy image pair," in *Proc. of Int. Conf. on Pattern Recognition*, pp. 1020–1024, IEEE, Stockholm, Sweden (2014).
- S. Osher and L. Rudin, "Feature-oriented image enhancement using shock filters," *SIAM J. Numer. Anal.* **27**(4), 919–940 (1990).
- L. Xu et al., "Image smoothing via L_0 gradient minimization," *ACM Trans. Graph.* **30**(6), 174 (2011).
- A. Levin et al., "Image and depth from a conventional camera with a coded aperture," *ACM Trans. Graph.* **26**(3), 70 (2007).
- Z. Wang et al., "Image quality assessment: from error visibility to structural similarity," *IEEE Trans. Image Process.* **13**(4), 600–612 (2004).
- W. S. Dong et al., "Compressive sensing via nonlocal low-rank regularization," *IEEE Trans. Image Process.* **23**(8), 3618–3632 (2014).

Shijie Sun is a PhD candidate in pattern recognition and intelligent systems at Shenyang Institute of Automation Chinese Academy of Sciences. He received his BS degree in aero-electronic countermeasure engineering and his MS degree in communication and information engineering from the PLA Air Force Engineering University in 2002 and 2007, respectively. His current research interests include image/video deblurring and processing.

Huaici Zhao is currently a professor at Shenyang Institute of Automation, Chinese Academy of Sciences. He received his BS and MS degrees in computer science and technology from Shandong University, Jinan, China, in 1996 and 1999 respectively, and his PhD in pattern recognition and intelligent systems from Shenyang Institute of Automation, Chinese Academy of Sciences, in 2003. His

research interests include complex system modeling and simulation, communication and signal processing, image processing.

Bo Li is a PhD candidate in pattern recognition and intelligent systems at Shenyang Institute of Automation, Chinese Academy of Sciences. He received his MS degree in computer application technology from Northeast Dianli University, Jilin, China, in 2006. His current research interests include image/video deblurring and processing.

Mingguo Hao is currently a senior engineer at Shenyang Institute of Automation, Chinese Academy of Sciences. He received his BS

degree in electromechanical engineering from Dalian University of Technology, Dalian, China, in 2000. His research interests include complex system modeling and simulation, image processing.

Jinfeng Lv is a PhD candidate in pattern recognition and intelligent systems at Shenyang Institute of Automation, Chinese Academy of Sciences. She received her BS degree in automation from Hunan University. Her research interests include image processing and artificial intelligence.